

# The Ising model on spherical lattices: dimer versus Monte Carlo approach

**O. Diego** <sup>\*</sup>, **J. González** <sup>†</sup>

*Instituto de Estructura de la Materia  
Serrano 123, 28006 Madrid  
Spain*

and

**J. Salas** <sup>‡</sup>

*Departamento de Física Teórica C-XI  
Universidad Autónoma de Madrid  
Cantoblanco 28049 Madrid  
Spain*

April 18, 2022

## Abstract

We study, using dimer and Monte Carlo approaches, the critical properties and finite size effects of the Ising model on honeycomb lattices folded on the tetrahedron. We show that the main critical exponents are not affected by the presence of conical singularities. The finite size scaling of the position of the maxima of the specific heat does not match, however, with the scaling of the correlation length, and the thermodynamic limit is attained faster on the spherical surface than in corresponding lattices on the torus.

---

<sup>\*</sup>e-mail: imtod67@cc.csic.es

<sup>†</sup>e-mail: imtjg64@cc.csic.es

<sup>‡</sup>e-mail: duncan@vm1.sdi.uam.es

# 1 Introduction

The Ising model conveys, in its simplicity, a richness of physical information which makes it relevant as a model for critical phenomena in different instances (ferromagnetic materials, lattice gas, binary alloys). The model is also paradigmatic of a common situation in statistical physics since, being one of the simplest models, yet it only allows to compute analytically the thermodynamic limit for particular classes of lattices (in one or two dimensions). In two dimensions, the Ising model in a square lattice has been solved in the continuum limit with cylindrical and toroidal boundary conditions [1, 2]. It has been also found analytic solution for the two-dimensional model on a triangular or honeycomb lattice [3]. In general, however, the introduction of more specific boundary conditions precludes the resolution of the model in closed analytic form.

On the other hand, when resorting to a numerical simulation of the observables one may take advantage of finite size effects to infer the critical behavior in the thermodynamic limit [4]. It happens, though, that finite size effects depend in general on the boundary conditions, in a way that may not be crucial but one cannot predict. There are again a few number of situations in which the asymptotic dependence on the spatial dimensions of the lattice has been rigorously studied. One of these cases corresponds to the analysis by Ferdinand and Fisher of the two-dimensional Ising model on large toroidal lattices [5]. The conclusions reached there support, in essence, the assumptions made in discussing finite size effects and, more precisely, the hypothesis of finite size scaling [6]. Some open questions are raised, however, regarding the approach to the critical coupling, which is drastically influenced by the shape of the torus.

The purpose of the present paper is to investigate finite size effects and critical properties of the Ising model on a class of two-dimensional lattices with spherical topology. Our choice for the elements of this class is not arbitrary, but is rather dictated by a prescription which makes possible increasing the size of the lattice without changing the local geometry. We propose to consider, in fact, a type of honeycomb lattices folded on the tetrahedron, which are built by assembling triangular blocks of the kind shown in Figure 1 as the faces of the polyhedron. One may construct a whole family of these lattices with increasing size, in such a way that the member of the  $N^{\text{th}}$  generation  $\Delta_n$  has a number of lattice points equal to  $n = 12N^2$ . The coordination number is constant in each lattice. Moreover, from the point of view of the simplicial geometry, the curvature is always concentrated at the same faces, which are those formed by the three-fold rings around the four vertices. In principle, this makes the problem of taking the thermodynamic limit along our sequence of lattices well-defined. In ref. [7] clear evidence was given of critical behavior in the ferromagnetic regime, as well as evidence supporting the hypothesis of finite size scaling applied to the model on the curved surface.

The lattices we are considering may be understood as the result of applying nontrivial boundary conditions for the honeycomb lattice on the plane, though they have the effect of introducing curvature in the model. We undertake the investigation of the influence of these boundary conditions on finite size effects and, more significantly from the physical point of view, on the critical properties of the model. Regarding the first point we will see that a discrepancy arises between the scaling of *pseudocritical* coupling constants for finite lattices and the true scaling of the correlation length. The second issue may be probably addressed in the continuum. In fact, investigations of the effect of boundary conditions in conformal field theories have been carried out before [8]. Anyhow, the inclusion of a conical singularity requires the kind of boundary condition which may call for a nonlocal operator in the theory [9], so the analysis of our model in the continuum does not appear quite straightforward.

The content of the paper is distributed as follows. In Section 2 we review the dimer approach applied to the computation of the partition functions and correlation functions of the model. Section 3 is devoted to the finite size analysis of data obtained with the above method, clarifying the issue concerning the  $\nu$  critical exponent. In Section 4 we give technical details of the Monte Carlo simulations carried out to measure in some of the larger lattices. Section 5 contains the results for the critical exponents  $\alpha, \beta, \gamma$  obtained after combining data from the dimer approach and the Monte Carlo simulations. Finally we draw our conclusions and outline further directions of our work.

## 2 The dimer approach to the Ising model

We review in this section the dimer formulation of the two-dimensional Ising model [10, 11]. This approach presents the advantage of being applicable to lattices with an irregular coordination. It allows to write partition functions and correlation functions in closed compact form, in terms essentially of determinants of some coordination matrices for the lattice. This is something that cannot be achieved for our curved lattices by any other standard resolution method of the two-dimensional Ising model. There is no obvious way, for instance, as to how to apply the transfer matrix method to write down the partition function for a lattice with the topology of the sphere, not even to produce a numerical computation of the same. Within the dimer approach one may, in principle, compute the partition function for any of the hexagonal lattices inscribed on the tetrahedron. Although we have not been able to infer from this construction the thermodynamic limit along the sequence of growing lattices, the method shows very efficient to calculate observables like the specific heat or the correlation length with arbitrary precision. One can easily progress to lattices with up to more than 1000 points, with the possibility of applying a finite size analysis to study the critical behavior of the model.

The dimer formulation of the Ising model makes use first of the equivalence between the partition function of the model and the dimer partition function of certain decorated lattice built from the original one [2]. One may apply afterward powerful techniques developed to perform the sum over dimer configurations. Let us review the former correspondence for the hexagonal lattice, while allowing for some kind of frustration which keeps constant the coordination number over the lattice. Given the collection of spins  $\{\sigma_i\}$ , with  $i$  running over all the lattice points, the partition function  $\mathcal{Z}$  is defined as the sum over all possible configurations

$$\mathcal{Z} = \sum_{\sigma_i = \pm 1} e^{-JH} \quad (1)$$

where the Hamiltonian  $H$  is given by the sum over all the lattice links  $\langle i, j \rangle$

$$H = - \sum_{\langle i, j \rangle} \sigma_i \sigma_j \quad (2)$$

The factor  $1/kT$  is absorbed for simplicity in the definition of the nearest-neighbor coupling  $J$ . It is well known that (1) can be cast as a sum over all the closed loops over the lattice. Calling this collection  $\{l_i\}$  and  $\{n_i\}$  the respective numbers of links of the paths, we have actually

$$\mathcal{Z} = (\cosh J)^l \sum_{\{l_i\}} (\tanh J)^{n_i} \quad (3)$$

$l$  being the total number of links of the lattice. One can draw a correspondence between each closed path and a dimer configuration in the appropriate decorated lattice. This is formed in our model by inserting a triangle in place of each of the points of the original lattice. To each of these one may assign four different states, depending on whether the point is traversed or not by a closed path and on what direction, in the first instance. These states are labeled in Figure 2. In a similar fashion, there are four different possible configurations of dimers on each triangle and adjacent links of the decorated lattice, which bear a one-to-one correspondence with the above states. These dimer configurations are labeled in Figure 3. One may easily convince that, establishing as a rule the equivalence between respective states in Figures 2 and 3, a unique closed path can be reconstructed starting from a given dimer configuration in the decorated lattice, and viceversa. Furthermore, if a weight equal to  $z = \tanh J$  is given to each dimer on a triangle link and equal to 1 for dimers joining neighboring triangles, it is clear that the dimer partition function reproduces the sum in the Ising partition function (3).

There exist, in turn, powerful techniques developed to the computation of dimer partition functions, which rely mainly on the relation between these and the Pfaffians of appropriate coordination matrices on the decorated lattice. We sketch here this relation, which has been worked out quite rigorously in ref. [11]. The first step is to establish an order relation among the points of the decorated lattice. Once this is done, one may assign a matrix element  $a_{p_1 p_2}$  for points numbered  $p_1$  and  $p_2$  such that  $a_{p_1 p_2} = \tanh J$  if the points belong to the same triangle,  $a_{p_1 p_2} = 1$  if they are nearest neighbors belonging to different

triangles, and  $a_{p_1 p_2} = 0$  otherwise. The sum over all dimer configurations weighted as proposed before amounts to perform the sum over all permutations  $\{p_1, p_2, \dots, p_K\}$ <sup>1</sup>

$$\sum a_{p_1 p_2} a_{p_3 p_4} \dots a_{p_{K-1} p_K} \quad (4)$$

restricted by  $p_1 < p_3 < \dots < p_{K-1}$  and  $p_1 < p_2, p_3 < p_4, \dots, p_{K-1} < p_K$ . While there is no known algorithm to compute efficiently a sum of the above kind, one may think of allowing for an antisymmetric matrix  $A = \{a_{ij}\}$ , so that the dimer partition function (a sum of all positive terms) may become proportional to

$$\sum (-1)^P a_{p_1 p_2} a_{p_3 p_4} \dots a_{p_{K-1} p_K} \quad (5)$$

with  $p_1 < p_3 < \dots < p_{K-1}$ ,  $p_1 < p_2, p_3 < p_4, \dots, p_{K-1} < p_K$ , as before, and  $(-1)^P$  being the signature of the permutation. The expression (5) reproduces the definition of the Pfaffian of the matrix  $A$ , which may be subsequently computed as the square root of its determinant. The remarkable conclusion which follows from the work of ref. [2] is that, for planar lattices, it is always possible to choose the sign of the nearest-neighbor matrix elements  $a_{p_1 p_2}$  so that all the terms in the sum (5) have the same sign. Since the matrix  $A$  becomes antisymmetric, it is customary to fix pictorially the sign of each  $a_{p_1 p_2}$  by giving an orientation to every link of the decorated lattice —  $a_{p_1 p_2}$  is positive, for instance, if the arrow goes from  $p_1$  to  $p_2$  —. We may enunciate the Kasteleyn theorem by saying that in any planar lattice there is always a system of arrows such that the dimer partition function can be computed as the Pfaffian of the corresponding antisymmetric coordination matrix.

The lattices we consider here fall into the category of planar lattices since they have the topology of the sphere. As long as we are interested on dimers mainly for computational purposes, we simply give the recipes which have to be followed to form the appropriate system of arrows on a planar lattice. Once superposed on the plane, the lattice is made of so-called elementary polygons, which are the closed cycles that do not contain points in their interior. On the other hand, a polygon is said to be clockwise odd if the number of arrows pointing in the clockwise direction in the polygon is odd. The basic results which hold for planar lattices are that (a) it is always possible to choose a system of arrows such that all the elementary polygons are clockwise odd, and (b) with this choice and taking  $a_{p_1 p_2}$  as positive when the arrow goes from  $p_1$  to  $p_2$ , all the terms in the expansion of the Pfaffian (5) have the same sign.

In our case, a possible system of arrows realizing the property (a) for a decorated lattice inscribed on the tetrahedron is shown in Figure 4, where all the arrows for the triangle links (not drawn) are supposed to point in the clockwise direction. The advantage of this choice of arrows is that it keeps a regular pattern in the bulk, while only a few arrows on the boundary links have to be flipped to make all elementary polygons clockwise odd. In general, progressing to the next member of our family of lattices on the tetrahedron just amounts to adding a column of (decorated) hexagons at each side of Figure 4, expanding appropriately the vertical dimension. The system of arrows proposed may be extended in a straightforward way to larger lattices. According to the above discussion, we set always the absolute value of matrix elements  $a_{p_1 p_2}$  equal to  $\tanh J$  for points in the same triangle, and equal to 1 for nearest neighbors on different triangles. The partition function for any honeycomb lattice on the tetrahedron can be represented, therefore, in terms of the respective matrix  $A$  by

$$\mathcal{Z} = (\cosh J)^l (\det A)^{1/2} \quad (6)$$

We have made use of the representation (6) to perform the numerical computation of the maximum of the specific heat (in the ferromagnetic regime) for lattices up to  $\Delta_{1452}$ . We have been able to measure that quantity with a relative error of less than  $10^{-7}$  in most of the cases. Correspondingly, a precise determination of the coupling constant at which the maximum is attained in each lattice has been also possible (see Table 1). The values of these pseudocritical coupling constants are fundamental ingredients for the finite size analysis to be accomplished in the next section. We have also computed the values of the specific heat of the curved lattices at the critical coupling constant of the planar honeycomb lattice (see Table 2). These are also relevant under the hypothesis of finite size scaling since, as we will see, the sequence of pseudocritical temperatures converges in the thermodynamic limit to the critical temperature of the planar hexagonal lattice.

---

<sup>1</sup> $K$  is the total number of points in the decorated lattice.

We conclude this section with an outline of how the two-point correlation functions can be obtained within the dimer approach [10, 11]. Given two arbitrary spins  $\sigma_p$  and  $\sigma_q$  in the lattice, the average

$$\langle \sigma_p \sigma_q \rangle = \frac{1}{\mathcal{Z}} \sum_{\sigma_i = \pm 1} \sigma_p \sigma_q e^{-JH} \quad (7)$$

may be computed with the following trick. One chooses a path  $\mathcal{C}$  from  $\sigma_p$  to  $\sigma_q$  on the lattice, which will comprise a number of consecutive spins  $\{\sigma_{p_1}, \sigma_{p_2}, \dots, \sigma_{p_m}\}$ . The two-point function may also be expressed as

$$\langle \sigma_p \sigma_q \rangle = \frac{1}{\mathcal{Z}} \sum_{\sigma_i = \pm 1} \sigma_p \sigma_{p_1} \sigma_{p_1} \sigma_{p_2} \dots \sigma_{p_{m-1}} \sigma_{p_m} \sigma_q e^{-JH} \quad (8)$$

Now we have that  $\sigma_p \sigma_{p_1}, \sigma_{p_1} \sigma_{p_2}, \dots, \sigma_{p_{m-1}} \sigma_{p_m}, \sigma_{p_m} \sigma_q$  are pairs of nearest-neighbor spins. Therefore, we find

$$\langle \sigma_p \sigma_q \rangle = \frac{1}{\mathcal{Z}} \sum_{\sigma_i = \pm 1} \prod_{\langle i, j \rangle \notin \mathcal{C}} (\cosh J + \sigma_i \sigma_j \sinh J) \prod_{\langle k, l \rangle \in \mathcal{C}} (\sinh J + \sigma_k \sigma_l \cosh J) \quad (9)$$

where the first product extends to all the links which do not belong to  $\mathcal{C}$ , and the second product runs over the links that do belong to the path. From (9) we arrive finally at the expression

$$\langle \sigma_p \sigma_q \rangle = \frac{1}{\mathcal{Z}} (\cosh J)^l (\tanh J)^{m+1} \sum_{\{l_i\}} (\tanh J)^{n_i - r_i} \frac{1}{(\tanh J)^{r_i}} \quad (10)$$

where the sum, as in expression (3), is over all the closed loops on the lattice, but with the difference now that the number  $r_i$  of links in each loop belonging to  $\mathcal{C}$  have to be weighted with  $(\tanh J)^{-1}$  rather than with  $\tanh J$ . It becomes obvious that all the machinery of the dimer formulation can be applied again to transform the sum in (10) into a suitable dimer partition function on the decorated lattice, so that

$$\langle \sigma_p \sigma_q \rangle = \frac{1}{\mathcal{Z}} (\cosh J)^l (\tanh J)^{m+1} (\det A')^{1/2} \quad (11)$$

The appropriate coordination matrix  $A' = \{a'_{ij}\}$  has to keep track of the different weight that the  $m+1$  links in  $\mathcal{C}$  carry in the sum over closed loops.

## 3 Finite size scaling and critical exponents

### 3.1 Finite size scaling

It is well known that singularities in the free energy (i.e. phase transitions) can only occur in the thermodynamic limit. For finite volumes the free energy is an analytic function of the temperature and any other parameter in the Hamiltonian. The thermodynamic singularities are thus smoothed out around the transition point. A trace of the existence of such non-analyticities is the presence of some peaks in the specific heat  $CV$  or magnetic susceptibility  $\chi$  curves. The dependence on the linear size of the system  $L$  of the location of the maxima of those peaks and their height permits the description of the thermodynamic limit from finite-size data [4].

In second order phase transitions this round-off is due to the fact that the correlation length  $\xi$  is limited by the size of the system. This fact defines a pseudocritical coupling  $J^*(L)$  such that

$$\xi(J^*(L)) \sim L \quad (12)$$

At this point the surface contribution to the free energy is not negligible compared to the bulk one. In the vicinity of a second order transition point  $J_c$  the correlation length diverges with a power-law given by

$$\xi(J) \sim (J - J_c)^{-\nu} \quad (13)$$

From (12) and (13) it can be derived the dependence of the pseudocritical coupling on the lattice size

$$|J^*(L) - J_c| \sim L^{-1/\nu} \quad (14)$$

Unfortunately in practical situations it is a very involved task to compute such quantity  $J^*(L)$ . It is easier to look at the position and height of those peaks mentioned above. If some quantity  $P$  diverges near the critical point as <sup>2</sup>

$$P(J) \sim |J - J_c|^{-\rho}; \quad \rho > 0 \quad (15)$$

then it can be shown [4] that for a finite volume it attains a maximum value  $P_{max}(J_L)$  at a point  $J_L(P_{max})$  given by

$$|J_L(P_{max}) - J_c| \sim L^{-\theta_P} \quad (16a)$$

$$P_{max}(J_L) \sim L^{\rho/\nu} \quad (16b)$$

when  $L$  is large enough. In most systems it is found that

$$\theta_P = \frac{1}{\nu} \quad (17)$$

but this is not a general result. There are some examples where this property does not hold: the spherical model, the ideal Bose gas [12] and the one-dimensional  $q = \infty$  clock model [13]. In the present paper we will face another situation in which the relation (17) is violated. On the other hand, if  $\theta \geq 1/\nu$  then the behavior of this quantity at finite volume evaluated at the critical point  $P_L(J_c)$  is the same as in (16b)

$$P_L(J_c) \sim L^{\rho/\nu} \quad (18)$$

Using (16a) and (16b) the critical coupling  $J_c$  and the critical exponents ratio  $\rho/\nu$  can be derived from finite-size data. When  $J_c$  is explicitly known and  $\theta_P \geq 1/\nu$  then (18) can be used instead of (16b). In this paper we are mainly concerned with the analysis of the susceptibility and the specific heat. So, we will obtain estimates of  $J_c$  and the ratios  $\gamma/\nu$  and  $\alpha/\nu$ . The rest of the critical exponents may be derived using the scaling relations [14]:

$$\frac{\beta}{\nu} = 1 - \frac{\gamma}{2\nu} \quad (19a)$$

$$\frac{1}{\nu} = 1 + \frac{\alpha}{2\nu} \quad (19b)$$

$$\eta = 2 - \frac{\gamma}{\nu} \quad (19c)$$

$$\delta = \frac{4}{\eta} - 1 \quad (19d)$$

However, in this paper we will check numerically scaling relations (19a) and (19b). We will obtain independent estimates of  $\nu$  and  $\beta/\nu$  respectively in terms of the analysis of the correlation length (see below) and the magnetization at the critical point (see Section 5).

### 3.2 Critical point and exponent $\theta_{CV}$

In Section 2 we showed that for lattices up to  $\Delta_{1452}$  we were able to obtain very accurate estimates of the internal energy  $E$  and the specific heat. These quantities are defined hereafter as follows

$$E_N = \frac{2}{3V} \langle H \rangle \quad (20)$$

$$CV_N = \frac{3V}{2} \sigma^2 \left( \frac{2}{3V} H \right) \quad (21)$$

where the factor  $3V/2$  is equal to the number of links in a lattice of  $V$  sites and  $\sigma(\cdot)$  is the standard deviation. Thus, the values of  $CV_{max}$  and  $J_L(CV_{max})$  can be computed with high precision. In what

---

<sup>2</sup>Hereafter we will denote quantities computed in a finite volume with a subscript  $L$  meaning the linear size of the system (i.e.  $P_L$ ). Whenever no subscript is present, the thermodynamic limit is assumed (i.e.  $P = \lim_{L \rightarrow \infty} P_L$ ).

follows we will identify the lattice linear size  $L$  with the index  $N$  characterizing the fullerene lattice (see Section 1). This choice is consistent as the volume increases as  $V = 12 N^2$ .

Data will be fitted according to Equation (16a)

$$J_N(CV_{max}) = J_c + AN^{-\theta_{CV}} \quad (22)$$

using a least  $\chi^2$  method. Here the input errors are given by the precision of the computer in calculating  $J_N(CV_{max})$ . In order to obtain a more reliable result, we will sequentially remove the point with smallest  $N$ . One eventually can observe a monotonous trend to some value, which will be identified with the thermodynamic limit.

Our best result is

$$J_c = 0.65850 \pm 0.00002 \quad (23)$$

for  $5 \leq N \leq 11$ . In this case  $\chi^2 = 0.07$  with 2 degrees of freedom. Throughout this paper all the errors associated with our final results will be equal to 2 standard deviations —i.e. 95% of confidence level—. The later result is compatible with the critical point of the Ising model on a toroidal honeycomb lattice

$$J_c^{\text{torus}} = \frac{1}{2} \log(2 + \sqrt{3}) = 0.65848 \quad (24)$$

This result can be easily derived using duality [14, 15]. Thus, our data strongly supports that both critical points coincide.

A good estimate of  $\theta_{CV}$  is obtained by repeating the fit with  $J_c = J_c^{\text{torus}}$ . The result is

$$\theta_{CV} = 1.745 \pm 0.015 \quad (25)$$

for  $6 \leq N \leq 11$  and with  $\chi^2 = 1.2$ . This one is in clear disagreement with the result expected for a lattice on a torus ( $\theta_{CV} = 1$  [5]). This fact makes necessary a direct determination of the  $\nu$  critical exponent, in order to see if the above measurement bears any relation to it (see below).

We will skip here the analysis of  $CV_{max}$ , as it is rather subtle to distinguish between a logarithmic and a power-law behaviors, specially when such a power is rather small. This will be carried out in Section 5.

### 3.3 Correlation length and exponent $\nu$

An independent way to compute the critical exponent  $\nu$  is to study the correlation length near the critical point. This quantity is defined in terms of the connected two-point function

$$\langle \sigma_{\mathbf{0}} \cdot \sigma_{\mathbf{r}} \rangle^c = \langle \sigma_{\mathbf{0}} \cdot \sigma_{\mathbf{r}} \rangle - \langle \sigma_{\mathbf{0}} \rangle \langle \sigma_{\mathbf{r}} \rangle \sim e^{-r/\xi} \quad (26)$$

when  $r$  is large enough. The connected two-point correlators are equal to the usual ones  $\langle \sigma_{\mathbf{0}} \cdot \sigma_{\mathbf{r}} \rangle$  for  $J < J_c$  (unbroken phase). This feature allows their exact computation using the machinery developed in Section 2. (For finite lattices odd quantities such as the magnetization are always equal to zero, even in the broken phase).

A major problem is how to recover  $\xi_N(J)$  from the finite-volume correlators  $\langle \sigma_{\mathbf{0}} \cdot \sigma_{\mathbf{r}} \rangle_N$ . For a torus of linear size  $L$  these functions are expected to behave as  $\sim \cosh((x - L/2)/\xi_L)$  when  $x \gg 1$ . But this question is not clear for the truncated tetrahedron. On the other hand, it is well known [11] that the correlation length does depend on the direction along the spins  $\sigma_{\mathbf{r}}$  are disposed. However, the same critical behavior is expected for all the possible directions.

This study has been carried out on the lattice  $\Delta_{972}$ , which is the largest one allowed by our computer facilities. We believe that this one is large enough to see the thermodynamic limit. We have chosen couples of spins along the diagonal in the representation on Figure 4 of the tetrahedron unfolded on the plane. Our choice for  $\sigma_{\mathbf{r}}$  allowed us to introduce an increasing distance between spins running from 3, 6, ... up to 27 (in units of the lattice spacing). At  $r = 27$  both spins are located at antipodal points. If we go on along the diagonal we finally arrive at  $\sigma_{\mathbf{0}}$ . For that reason we expect that the correlators behave for large  $r$  as a symmetrized version of equation (26). In order to improve our results, we include in our ansatz the correct leading term for the square lattice on the torus [11]

$$\langle \sigma_{\mathbf{0}} \sigma_{\mathbf{r}} \rangle = \frac{f}{\sqrt{r}} e^{-r/\xi} (1 + \mathcal{O}(1/r)) \quad (27)$$

suitably symmetrized around  $r = 27$ .

We have analyzed the cases  $J = 0.58, 0.59, 0.60, 0.61$  and  $0.62$  (see Table 3 and Figure 5). We have obtained extremely good fits for all these cases, giving differences of order  $\sim 10^{-5}$ . Although the lattice  $\Delta_{972}$ , as any of the lattices inscribed on the tetrahedron, is not homogeneous, it is remarkable that the values of the two-point functions at each different  $J$  fit, to a high degree of precision, to the correct leading behavior for the Ising model on a square lattice on the torus. The deviation that we have found from the dependence (27) appears to be even smaller than for similar measurements carried out for the lattice on a torus. The estimated values of the correlation length are shown in Table 3 and will be used in the computation of the  $\nu$  critical exponent. We unsuccessfully tried to fit data for  $J > 0.62$  to (27). The reason is that very close to the critical point we have to take into account in Equation (27) the  $\mathcal{O}(1/r)$  (or even higher) terms.

Given the values of  $\xi_{N=9}^{-1}(J)$  in Table 3, we tried to fit them according to (13)

$$\xi_{N=9}^{-1}(J) = A|J - J_c|^\nu \quad (28)$$

We obtain a value equal to  $\nu = 1.01 \pm 0.04$  with  $\chi^2 = 0.36$ . However, if we drop the point with  $J = 0.62$  (the closest to  $J_c$ ) the result is

$$\nu = 1.00 \pm 0.06 \quad (29)$$

with a remarkable small value of the  $\chi^2 \sim 7 \cdot 10^{-5}$ .

The conclusions of the analysis of the data coming from the dimer computations can be summarized in the following points (a) The critical point is compatible with  $J_c^{\text{torus}}$ . (b) The critical exponent  $\nu = 1.00 \pm 0.06$ . (c) The finite-size exponent  $\theta_{CV} = 1.745 \pm 0.015$  is significantly different from  $1/\nu$ . In summary, our results suggest that the critical properties of the Ising model on the truncated tetrahedron are the same as on the torus. However, we find a very clear difference in the finite-size behavior of those models, as long as the scaling of pseudocritical coupling constants (determined from the maxima of the specific heat) does not match with the scaling behavior of the correlation length. On the tetrahedron the thermodynamic limit is achieved much faster than on the torus, at least in what concerns to the specific heat.

## 4 Technical aspects of the Monte Carlo simulations

We have performed several Monte Carlo (MC) runs for different lattice volumes  $V = 12N^2$  and coupling constants  $J$ . The relevant information about the simulations can be found in Table 4.

We have used a Metropolis algorithm with the R250 pseudorandom-number generator [16] –initialized with the RANMAR subroutine–. The period of such generator is equal to  $2^{250} - 1$ . Recently, it has been claimed [16] that the combination of the Metropolis algorithm with the R250 generator gives better results than other more involved procedures. We have compared those values obtained both by the dimer approach and by direct MC simulation. They were consistent within statistical errors.

In all cases we have measured the internal energy density and the magnetization defined as

$$M_N = \left\langle \left| \frac{1}{V} \sum_i \sigma_i \right| \right\rangle \quad (30)$$

We have also measured the specific heat and the magnetic pure-phase susceptibility,

$$\chi_N = V\sigma^2 \left( \left| \frac{1}{V} \sum_i \sigma_i \right| \right) \quad (31)$$

In all cases we discarded the first  $10^5$  MC steps for thermalization. Then we have measured each observable once every typically 100 MC steps. In this way we obtained statistically independent data, as it can be checked by computing the corresponding autocorrelation times [17].

In order to calculate the maximum value of the specific heat and the susceptibility we have used the Spectral Density Method [18]. At a given coupling  $J$  we can obtain the histograms  $N(E, M; J)$  which keep track of the numbers of configurations with magnetization  $M$  and internal density energy  $E$ . This



information is enough in order to compute the expectation value of any function  $f(M, E)$  at any other coupling  $J'$ . In our case the magnetic field is zero and in the equations (20,21,30,31) the observables do not depend on  $E$  and  $M$  simultaneously. For those reasons we could use the following formulae

$$\langle f(E) \rangle(J') = \frac{\sum_E f(E) N_0(E; J) \exp\{(J' - J)E\}}{\sum_E N_0(E; J) \exp\{(J' - J)E\}} \quad (32)$$

$$\langle f(M) \rangle(J') = \frac{\sum_E N_f(E; J) \exp\{(J' - J)E\}}{\sum_E N_0(E; J) \exp\{(J' - J)E\}} \quad (33)$$

where the one dimensional histograms are defined as follows

$$N_0(E; J) = \sum_M N(E, M; J) \quad (34)$$

$$N_f(E; J) = \sum_M f(M) N(E, M; J) \quad (35)$$

The Spectral Density Method gives the correct answer for couplings  $J'$  close to the coupling  $J$  where the simulation was performed. A criterion for the applicability of such method is the following [18]

$$|J' - J| \sim \frac{1}{\sigma(E)V} \quad (36)$$

In most cases only one simulation at  $J = J_c$  is enough in order to determine the maximum of  $CV$  and  $\chi$ . However, for the smaller lattices an additional run had to be performed in order to obtain a reliable estimate of such quantities.

We have divided up the entire sample into typically 30–120 subsamples, each of them containing  $\sim 1000$  measures. For each subsample we computed every quantity (including  $CV_{max}$ ,  $J_N(CV_{max})$ , ...). With these estimates we calculated the statistical errors using the jack-knife method [19]. In this way, the effect of correlation among data was taken into account.

We have done all the MC simulations on a VAX 9000 machine with a vectorial processor. The program was not fully vectorizable, as the lattice could not be splitted into two disjoint sublattices, in such a way every element of one sublattice is surrounded by elements belonging to the other one<sup>3</sup>. However, we could divide the whole lattice into three subsets. The elements of the first two are arranged on two disjoint triangular sublattices, so their update could be fully vectorize. On the other hand, the rest of the spins can be located on two lines joining pairs of vertices on the tetrahedron and their number depend explicitly on the planar representation of the lattice. For these ones the update is clearly not vectorizable. However, their effect on the CPU time is not very important for the larger lattices, as their number behaves as  $\sim V^{1/2}$ .

## 5 Results of the Monte Carlo simulations

### 5.1 Position of the critical point

Here we will repeat the analysis of Section 3, but with all the data of Table 1. For data coming from the dimer analysis the input error will be taken as the precision of the subroutines used. For those coming from the MC simulations the error is given by the jack-knife method described in the preceding section. Data for  $N > 11$  posses large error bars compared with the rest. For that reason the fits presented in Section 3 cannot have large variations. Our final results for the specific heat are

$$J_c = 0.65850 \pm 0.00002 \quad (37)$$

for  $5 \leq N \leq 21$  and with  $\chi^2 = 0.67$ . And

$$\theta_{CV} = 1.745 \pm 0.015 \quad (38)$$

---

<sup>3</sup>This feature has to do with the onset of frustration in the antiferromagnetic regime.

for  $6 \leq N \leq 21$  and with  $\chi^2 = 1.9$  (See Figure 7).

If we repeat the same procedure with the susceptibility we obtain an estimate for  $J_c$  compatible with the later one, but with larger error bar. If we fix this quantity to  $J_c^{\text{torus}}$  we arrive at the following estimate for the exponent  $\theta_\chi$

$$\theta_\chi = 1.01 \pm 0.02 \quad (39)$$

for  $9 \leq N \leq 21$  and  $\chi^2 = 0.8$  (See Figure 7).

We observe that  $\theta_\chi$  is close the value  $1/\nu = 1$ , in agreement with the Ising model on the torus. We conclude that

$$\frac{1}{\nu} = \theta_\chi < \theta_{CV} \quad (40)$$

and this feature implies that one can obtain the critical exponents using either eq. (16b) or eq. (18). As we have identified the critical coupling of our system, it seems more natural to rely our conclusions on eq. (18). In any case, the values obtained from eq. (16b) are always consistent with those presented in this paper within statistical errors.

## 5.2 Exponent ratios $\gamma/\nu$ and $\beta/\nu$

The value of  $\gamma/\nu$  can be derived using the value of the critical magnetic susceptibility  $\chi_N(J_c)$ . We have fitted our data to

$$\chi_N(J_c) = AN^{\gamma/\nu} \quad (41)$$

and our best result is

$$\frac{\gamma}{\nu} = 1.73 \pm 0.02 \quad (42)$$

for values of  $N$  ranging from 21 to 9 and with  $\chi^2 = 0.79$  This result is very close to the usual Ising model one  $\gamma/\nu = 7/4 = 1.75$ . If we fix  $\gamma/\nu$  to this value we obtain a  $\chi^2$  value of  $\sim 2.8$  which shows that the fit is reasonably good (See Figure 8).

To determine the value of  $\beta/\nu$  in an independent way (i.e. not using scaling relation (19a)) we will fix our attention on the magnetization at the critical point. In the thermodynamic limit the magnetization near  $J_c$  behaves as

$$M(J) \sim |J - J_c|^\beta \quad (43)$$

Using similar arguments as in Section 3 it can be predicted that

$$M_N(J_c) \sim N^{-\beta/\nu} \quad (44)$$

The result of performing such fit is the following

$$\frac{\beta}{\nu} = 0.126 \pm 0.004 \quad (45)$$

using data with  $7 \leq N \leq 21$  and with  $\chi^2 = 0.33$  (See Figure 9). This value is also very close to the Ising one  $\beta/\nu = 1/8 = 0.125$ . This result supports that the scaling relation (19a) does hold in this model.

This feature can be used in order to obtain a more accurate estimate of those exponents. We can try to fit  $\chi_N(J_c)$  and  $M_N(J_c)$  simultaneously using explicitly the relation (19a). The result is

$$\begin{aligned} \gamma/\nu &= 1.748 \pm 0.008 \\ \beta/\nu &= 0.126 \pm 0.004 \end{aligned} \quad (46)$$

Thus, our results strongly suggest that the ratio  $\gamma/\nu = 7/4$  as in the Ising model on a torus. Notice that the error in that ratio is less than 0.6%. Using the relations (19c) and (19d) we can derive the value of the exponents  $\eta$  and  $\delta$ .

$$\eta = 2 - \frac{\gamma}{\nu} = 0.252 \pm 0.008 \quad (47a)$$

$$\delta = \frac{4}{\eta} - 1 = 14.8 \pm 0.6 \quad (47b)$$

### 5.3 Exponent ratio $\alpha/\nu$

We can perform the same game for the specific heat and try to obtain the exponent ratio  $\alpha/\nu$ . If we try to fit data to the function

$$CV_N(J_c) = A + BN^{\alpha/\nu} \quad (48)$$

we do not obtain a satisfactory result. The best one gives a ratio  $\alpha/\nu \sim 0.060$  with  $\chi^2 \sim 9$  and  $9 \leq N \leq 21$  (See Figure 8). On the other hand, and motivated in part for the preceding results we could try to fit the data to a logarithmic function.

$$CV_N(J_c) = A + B \log N \quad (49)$$

In this case, the fit is successful giving a  $\chi^2 = 1.9$  with  $7 \leq N \leq 21$  (See Figure 10). This immediately implies that

$$\alpha = 0 \quad (50)$$

and using equation (19b)

$$\nu = 1 \quad (51)$$

which is in agreement with the result from direct measurements of the correlation length displayed in Section 3. Thus, both exponents take the same values as in the Ising model on the torus. On the other hand, we have also verified that the scaling relation (19b) does hold in this model.

## 6 Conclusions and outlook

In this paper we have presented the first deep study of the critical properties of an Ising model on a lattice with the topology of the sphere. In particular we have chosen the family of honeycomb lattices that can be constructed on the tetrahedron. Our results can be summarized as follows

- The dimer approach is very useful and competitive for lattices up to  $\sim 10^3$  points. It provides very accurate data for the internal energy, specific heat and two-point correlators.
- The critical properties of the Ising model on the tetrahedron are just the same as on the torus. In particular we have checked that  $J_c$  is the same, as well as the critical exponents  $\nu$ ,  $\alpha$ ,  $\gamma$  and  $\beta$ .
- We also have checked two scaling relations (19a) and (19b) among these exponents. Using the two other equations we obtained the last two critical exponents  $\delta$  and  $\eta$ . They are in agreement with those corresponding to the Ising model on a torus.
- But the finite-size scaling properties of those two systems are not the same. In our case the position of the maxima of the specific heat scales near  $J_c$  with a critical exponent that does not bear any relation to the critical behavior of the correlation length. That is, the thermodynamic limit is achieved faster on the tetrahedron. However, the behavior of the susceptibility is just the same in both ones.

Our results suggest that the same analysis carried out in other types of lattices with the same topology will yield the same conclusions: the critical behavior does not change, although variations in their finite-size properties are expected to hold. All of them belong to the same universality class of the Ising model on a torus.

On the other hand, the Ising model on the tetrahedron can be view as the Ising model with some non-standard boundary conditions. These ones has the advantage that the critical behavior is reached before than for periodic boundary conditions.

Ferdinand and Fisher [5, 4] studied how the exponent  $\theta_{CV}$  varies for the Ising model defined on a square lattice on a  $m \times n$  torus. They concluded that  $J_l(CV_{max})$  behaves as

$$\frac{J_l(CV_{max})}{J_c^{\text{torus}}} = 1 + \frac{b(\eta)}{l} + o(l^{-1}) \quad (52)$$

where  $l = (m^{-2} + n^{-2})^{-1}$  measures the linear size of the torus and  $\eta = m/n$  its shape. They also showed that  $b(\eta)$  is not a monotonous function of  $\eta$ . In particular  $b(\eta) > 0$  in the range  $\eta \in (\eta_0^{-1}, \eta_0)$  with  $\eta_0 = 3.139278$ , and  $b(\eta) < 0$  in  $\eta \in (0, \eta_0^{-1}) \cup (\eta_0, \infty)$ . Exactly at  $\eta = \eta_0$  and  $\eta_0^{-1}$  the function  $b(\eta)$  vanishes<sup>4</sup>, so at these points the leading term in (52) vanishes and its behavior is controlled by the subleading term. In this model it can be written as

$$\frac{J_l(CV_{max})}{J_c^{\text{torus}}}\Big|_{\eta=\eta_0} = 1 - \frac{c \log l}{l^2} + \dots \quad (53)$$

The behavior of  $b(\eta)$  as a function of the shape of the torus is explained as a highly non-trivial interplay between the different terms which appear in the expression of the partition function. We believe that the same feature is present in the Ising model on the truncated tetrahedron. In this case, the shape of the lattice is fixed, but the chosen boundary conditions are the basic ingredient which makes the leading term in (52) vanish.

We should mention that our conclusions may not apply to the antiferromagnetic regime. The reason is that for such boundary conditions, the lattice is not bipartite. Thus, the phenomenon of frustration may occur in that regime. This feature is absent in the Ising model on the torus. In this case, the lattice is bipartite and for sufficiently low temperatures we find a Néel ground state. This question on the tetrahedron is currently under research.

Finally, we would like to say a few words about the continuum theory which is attained in the thermodynamic limit. The evidence we have found of scaling suggests a description in terms of the fields and weights of a conformal field theory. This cannot be a trivial example of field theory on the sphere (or on the plane), since four curvature singularities arise which cannot be removed by conformal transformations. Under the assumption of conformal invariance, though, we could still stick three of the vertices together (at a point we may take as infinity) by means of  $SL(2, C)$  transformations, leaving alone a singularity in the bulk. This picture is close in spirit to the Coulomb gas representation of conformal field theories, but with the difference now that not all the curvature is pinched at the point at infinity. A conical singularity on the plane may have sensible effects on the correlation functions of the theory. We recall here another example with nontrivial boundary conditions, namely that of a conformal field theory on the semiplane. In this case correlators which are taken at a finite distance of the boundary do not measure the conformal weights of the theory on the plane [20]. In our model, it may not be necessary to compute correlators infinitely far away from the singularity to measure bulk conformal weights, but again some dependence on the location of the points should be expected. This point should deserve further clarification, though its investigation in the lattice would require more powerful computer facilities than used in the present work.

## Acknowledgements

We thank Juan Jesús Ruiz-Lorenzo and Miguel Angel Martín-Delgado for helpful discussions. We acknowledge the financial support of the CICyT.

---

<sup>4</sup>The same occurs for  $\eta = 0, \infty$  [5]

# References

- [1] L. Onsager, Phys. Rev. **65** (1944) 117.
- [2] P.W. Kasteleyn, J. Math. Phys. **4** (1963) 287.
- [3] R.M.F. Houtappel, Physica **16** (1950) 425.  
K. Husimi and I. Syozi, Prog. Theor. Phys. **5** (1950) 177.  
G.H. Wannier, Phys. Rev. **79** (1950) 357.  
J. Stephenson, J. Math. Phys. **5** (1964) 1009.
- [4] M.N. Barber, *Finite-size Scaling in Phase Transitions and Critical Phenomena*, vol. 8, edited by C. Domb and J.L. Lebowitz. (Academic Press, New York, 1983).
- [5] A.E. Ferdinand and M.E. Fisher, Phys. Rev. **185** (1969) 832.
- [6] M. E. Fisher, *Critical Phenomena*, Proceedings of the Enrico Fermi Summer School, edited by M. S. Green (Academic Press, New York, 1971).  
M. E. Fisher and M. N. Barber, Phys. Rev. Lett **28** (1972) 1516.
- [7] J. González and M.A. Martín-Delgado, “Exact Finite-Size Results on the Ising model in 2D Curved Space”, PUP-T-1367 preprint. Bulletin board hep-th/9301057.
- [8] J.L. Cardy, Nucl. Phys. **B229** (1987) 355.  
J.L. Cardy and I. Peschel, Nucl. Phys. **B300** (1988) 377.  
J.L. Cardy and D.C. Lewellen, Phys. Lett. **B259** (1991) 274.  
J.L. Cardy, J. Phys. **A17** (1984) L385.
- [9] D. Polyakov, “Curvature Singularity as the Vertex Operator”, Rutgers preprint RU-92-63 (December 1992). Bulletin board hep-th/9302017.
- [10] E. W. Montroll, *Lectures on the Ising Model of Phase Transitions* in Brandeis University Summer Institute in Theoretical Physics 1966, edited by M. Chrétien, E. P. Gross and S. Deser (Gordon and Breach, New York, 1968).
- [11] B.M. McCoy and T.T. Wu, *The Two-Dimensional Ising Model* (Harvard University Press, 1973).
- [12] M.E. Fisher and M.N. Barber, Ann. Phys. **77** (1973) 10.  
M.N. Barber, Aust. J. Phys. **26** (1973) 483.
- [13] M. Asorey, J.G. Esteve and J. Salas, “Finite Size Analysis of the One-dimensional  $q = \infty$  Clock Model”, preprint DFTUZ 93.3. Bulletin board hep-lat/9306022.
- [14] C. Itzykson and J.-M. Drouffe, *Statistical Field Theory*, Vol. 1 (Cambridge University Press, Cambridge, 1989).
- [15] R.J. Baxter, *Exactly Soluble Models in Statistical Mechanics*, (Academic Press, 1990).
- [16] A.M. Ferrenberg, D.P. Landau and Y.J. Wong, Phys. Rev. Lett. **69** (1992) 3382.  
I. Vattulainen, K. Kankaala, J. Saarinen and T. Ala-Nissila, “A Comparative Study of Some Pseudorandom Number Generators”, preprint HU-TFT-93-22, Bulletin board hep-lat/9304008.
- [17] A.D. Sokal, *Monte Carlo Methods in Statistical Mechanics: Foundations and New Algorithms* in “Cours de la Troisième Cycle de la Physique en Suisse Romande”, June 1989 Lausanne.  
U. Wolff, Phys. Lett. **B228** (1989) 379.
- [18] M. Falcioni *et al.*, Phys. Lett. **B108** (1982) 331.  
A. M. Ferrenberg and R. H. Swendsen, Phys. Rev. Lett. **61**, 2635 (1988); **63**, 1195 (1989).

[19] M. Fukugita, M. Okawa and A. Ukawa, Nucl. Phys. **B337** (1990) 181.

[20] J.L. Cardy, Nucl. Phys. **B240** (1984) 514.

# Figure Captions

**Figure 1:** Generic triangular block for honeycomb lattices embeded on the tetrahedron.

**Figure 2:** Different paths through a honeycomb lattice site.

**Figure 3:** Dimer configurations around a triangle of the decorated lattice.

**Figure 4:** Decorated lattice for the second generation. The outer lines show the identifications of boundary links which embed the lattice on the tetrahedron.

**Figure 5:** Values of the unsubtracted two-point correlators  $\langle \sigma_{\mathbf{r}} \sigma_{\mathbf{0}} \rangle$  for different separations  $r$  and couplings constants  $J = 0.57, 0.58, \dots, 0.62$ . The least  $\chi^2$  fits are also depicted.

**Figure 6:** Values of  $\xi(J)^{-1}$  for those  $J$  listed in Table 3. The straight line corresponds to the  $\chi^2$  fit.

**Figure 7:** Values of the position of the maxima of the specific heat (circles) and the magnetic susceptibility (squares) with respect to the critical coupling  $J_c^{\text{torus}}$ . The power-law fits are also depicted.

**Figure 8:** Power-law fits of the values of the specific heat (squares) and the magnetic susceptibility (circles) at the critical point  $J_c$ .

**Figure 9:** The same as in Figure 8 for the magnetization  $M_N(J_c)$ .

**Figure 10:** Logarithmic least  $\chi^2$  fit to  $CV_N(J_c)$ .

## Table Captions

**Table 1:** For each lattice size  $N$  we show the values of the maximum of the specific heat and the position of such point  $(CV_{max}, J_N(CV_{max}))$  and the same for the susceptibility  $(\chi_{max}, J_N(\chi_{max}))$ . Those values marked with a  $\dagger$  were computed using the exact partition function [7], those with a  $\ddagger$  using the dimer approach (see Section 2) and those with an  $\star$  by evaluating exactly (and numerically) the partition function. The rest were obtained by means of the Monte Carlo simulations described in Section 3.

**Table 2:** For each lattice size  $N$  we show the values of the specific heat  $CV_N(J_c)$ , the susceptibility  $\chi_N(J_c)$  and the magnetization  $M_N(J_c)$  evaluated at the critical point  $J_c^{\text{torus}}$ . The symbols possess the same meaning as in Table 1.

**Table 3:** Values of the inverse of the correlation length computed for the  $N = 9$  lattice and different values of the coupling  $J$ .

**Table 4:** Number of Monte Carlo steps performed for each simulation in a lattice of volume  $V = 12N^2$  and coupling constant  $J$ .



$N$	$CV_{max}$	$J_N(CV_{max})$	$\chi_{max}$	$J_N(\chi_{max})$
1	1.43923551(1) <sup>†</sup>	0.467332(1) <sup>†</sup>	1.2564278(1) <sup>*</sup>	0.487805(1) <sup>*</sup>
2	1.65204595(1) <sup>†</sup>	0.608224(1) <sup>†</sup>		
3	1.89238232(1) <sup>†</sup>	0.634238(1) <sup>†</sup>	7.91(2)	0.6215(3)
4	2.07977738(1) <sup>‡</sup>	0.643862(1) <sup>‡</sup>		
5	2.23081551(1) <sup>‡</sup>	0.648580(1) <sup>‡</sup>	18.98(7)	0.6377(3)
6	2.35682745(1) <sup>‡</sup>	0.651275(1) <sup>‡</sup>		
7	2.46477396(1) <sup>‡</sup>	0.652973(1) <sup>‡</sup>	34.4(1)	0.6444(2)
9	2.64288048(1) <sup>‡</sup>	0.654929(1) <sup>‡</sup>	53.3(2)	0.6480(2)
11	2.786536(6) <sup>‡</sup>	0.65598(5) <sup>‡</sup>	75.9(4)	0.6498(2)
15	3.02(1)	0.6571(3)	128.4(8)	0.6523(2)
21	3.30(2)	0.6579(3)	232(2)	0.6540(2)

**Table 1**

$N$	$CV_N(J_c)$	$\chi_N(J_c)$	$M_N(J_c)$
1	0.99350489(1) <sup>†</sup>	0.8617020(1) <sup>*</sup>	0.82868806(1) <sup>*</sup>
2	1.51639951(1) <sup>†</sup>		
3	1.81746516(1) <sup>†</sup>	6.889(3)	0.6904(9)
5	2.19465654(1) <sup>‡</sup>	16.89(9)	0.645(1)
6	2.32898639(1) <sup>‡</sup>		
7	2.44249002(1) <sup>‡</sup>	30.8(1)	0.6168(7)
9	2.62744012(1) <sup>‡</sup>	48.2(3)	0.597(1)
11	2.77(1)	68.3(4)	0.5828(9)
15	2.998(9)	116(1)	0.560(1)
21	3.24(1)	210(2)	0.536(2)

**Table 2**

$J$	$\xi_{N=9}^{-1}$
0.57	0.204(7)
0.58	0.181(5)
0.59	0.158(1)
0.60	0.135(2)
0.61	0.112(1)
0.62	0.088(1)

**Table 3**

$N$	$J$	MC steps
3	$J_c^{\text{torus}}$	$3 \cdot 10^6$
3	0.62	$3 \cdot 10^6$
5	$J_c^{\text{torus}}$	$3 \cdot 10^6$
5	0.64	$3 \cdot 10^6$
7	$J_c^{\text{torus}}$	$12 \cdot 10^6$
9	$J_c^{\text{torus}}$	$12 \cdot 10^6$
11	$J_c^{\text{torus}}$	$12 \cdot 10^6$
15	$J_c^{\text{torus}}$	$11 \cdot 10^6$
21	$J_c^{\text{torus}}$	$12 \cdot 10^6$

**Table 4**

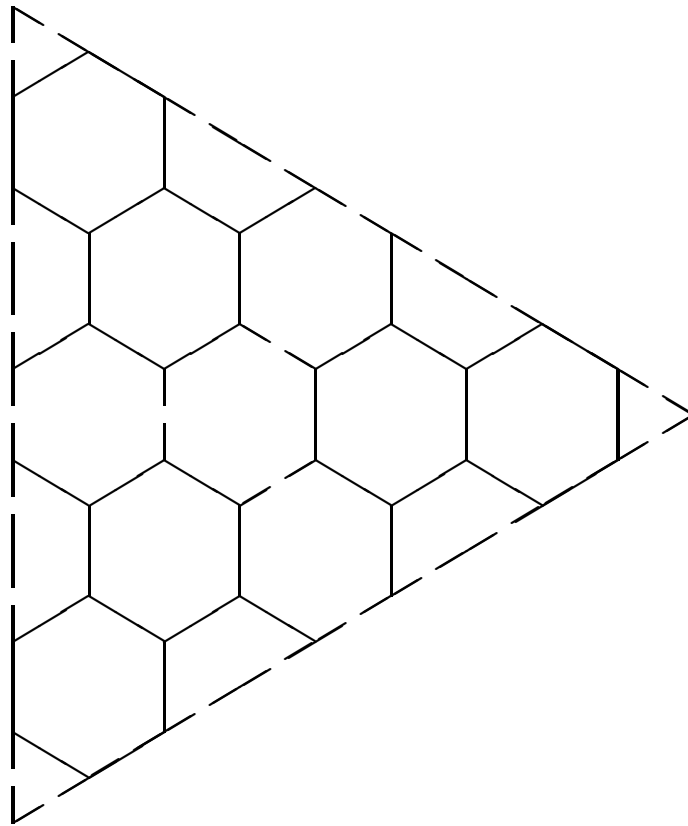
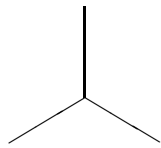
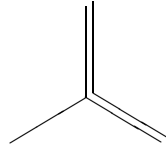


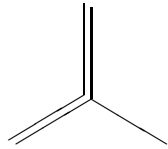
Figure 1:



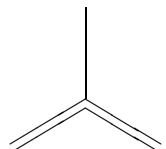
(a)



(b)

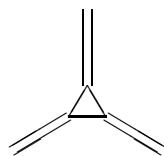


(c)

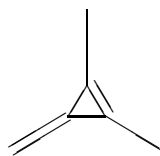


(d)

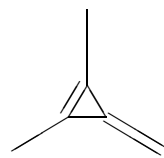
Figure 2:



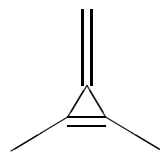
(a)



(b)



(c)



(d)

Figure 3:

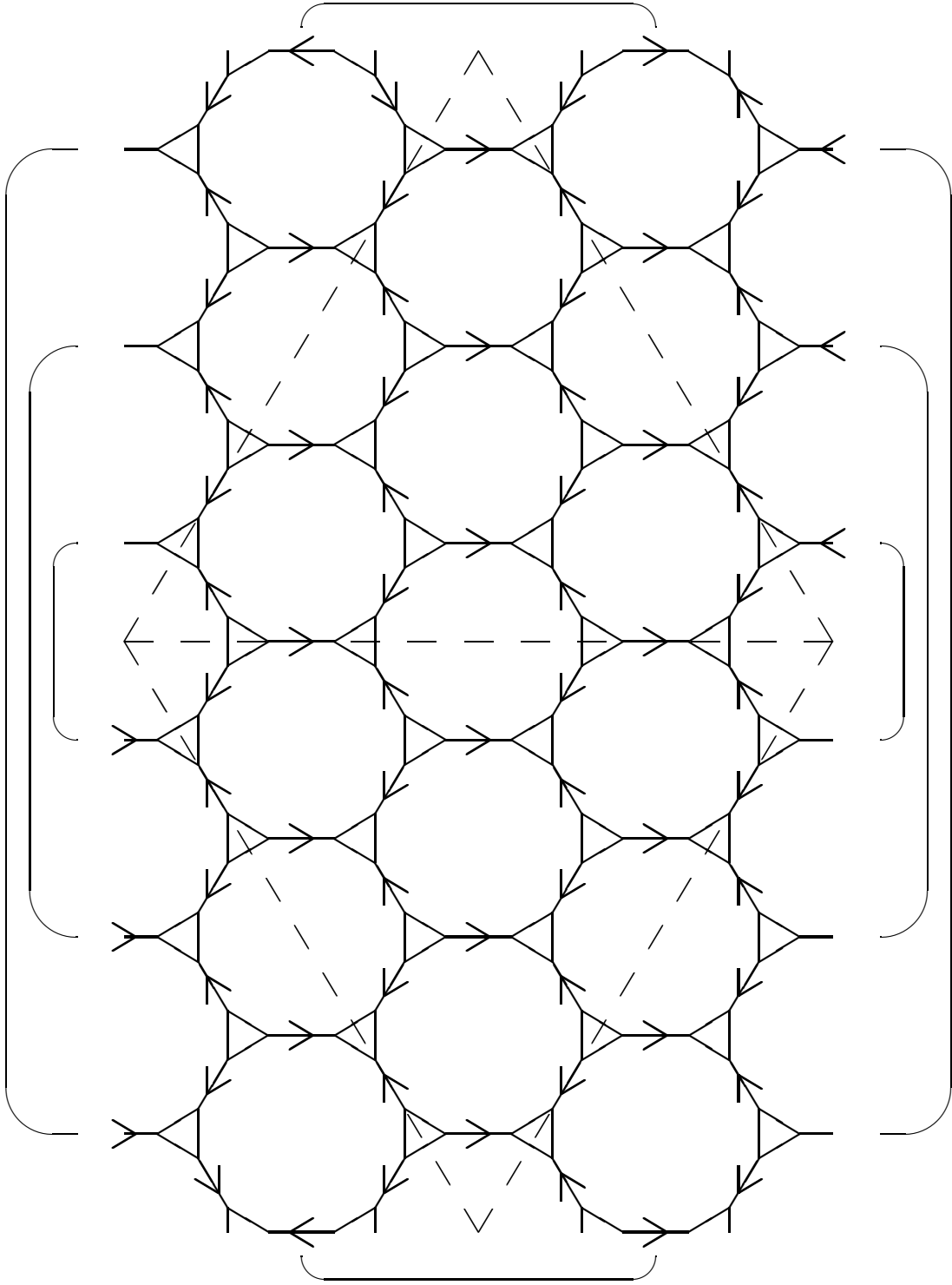


Figure 4: